SPECTROSCOPY OF GRB 050505 AT $z = 4.275$: A log N(H I) = 22.1 DLA HOST GALAXY AND THE NATURE OF THE PROGENITOR

E. BERGER,[1,2,3] B. E. PENPRASE,[4] S. B. CENKO,[5] S. R. KULKARNI,[6] D. B. FOX,[7] C. C. STEIDEL,[6] AND N. A. REDDY[6]

ABSTRACT

We present optical spectroscopy of the afterglow of GRB 050505 obtained with the Keck I 10 m telescope. The spectrum exhibits three absorption systems with the highest, at $z = 4.2748$, arising in the host galaxy. The host absorption is marked by a DLA with log N(H I) = 22.05 ± 0.10, higher than that of any QSO-DLA detected to date but similar to several other recent measurements from GRB spectra. We further deduce a metallicity of $Z \approx 0.06\ Z_\odot$, with a depletion pattern that is similar to that of the Galactic warm halo or warm disk. More importantly, we detect strong absorption from Si II* indicating a dense environment, $n_H \gtrsim 10^2\ cm^{-3}$, in the vicinity of the burst, with a size of ∼4 pc. The C IV absorption system spans a velocity range of about $10^3\ km\ s^{-1}$, most likely arising in the progenitor stellar wind. In this context the lack of corresponding Si IV absorption indicates that the progenitor had a mass $\lesssim 25\ M_\odot$ and a metallicity $\lesssim 0.1\ Z_\odot$, and therefore required a binary companion to eject its hydrogen envelope prior to the GRB explosion. Finally, by extending the GRB-DLA sample to $z \approx 4.3$ we show that these objects appear to follow a similar metallicity-redshift relation as in QSO-DLAs, but with systematically higher metallicities. It remains to be seen whether this trend is simply due to the higher neutral hydrogen columns in GRB-DLAs and/or sight lines which probe star-forming regions, or if it is a manifestation of different star formation properties in GRB-DLAs.

Subject headings: gamma rays: bursts — ISM: abundances — ISM: kinematics and dynamics — stars: mass loss — stars: Wolf-Rayet

1. INTRODUCTION

The study of star formation and the associated production and enrichment of the interstellar medium (ISM) and intergalactic medium (IGM) by metals is focused on two observational approaches: large galaxy surveys based on rest-frame UV, optical, near-infrared, and far-infrared emission, and the use of high-redshift quasars as probes of the ISM/IGM. The former provides a view of the star formation activity from high redshift to the present, as well as the possible enrichment of the IGM through galactic-scale winds. In the context of quasar absorption studies the highest column density absorbers, the so-called damped Lyα (DLA) systems [N(H I) $\geq 2 \times 10^{20}\ cm^{-2}$] are of particular interest. This is because of the similarity of their column densities to those in local luminous galaxies, the fact that at these columns the hydrogen is mainly neutral and may form stars, and the conclusion that the bulk of the neutral gas in the range $z \sim 0$–5 is in DLAs (for a recent review see Wolfe et al. 2005 and references therein).

The connection between luminous star-forming galaxies and DLAs remains an open question. This is primarily due to observational limitations inherent in both approaches. First, surveys of star-forming galaxies at $z \gtrsim 2$ are limited to relatively bright objects, $L \gtrsim 0.3L^*$ (e.g., Steidel et al. 2003). Furthermore, with the exception of the brightest galaxies, the continuum emission is typically too faint for absorption from interstellar gas to be observed and therefore for it to be possible to tie together the star formation and ISM properties. On the other hand, the use of quasar sight lines to probe the disks of high-redshift galaxies is biased by a cross section selection effect to large impact parameters ($\gtrsim 10$ kpc). Moreover, in the particular case of DLAs the close proximity on the sky to the bright background quasar severely limits the identification of the DLA counterparts. Thus, while some DLA counterparts have been identified, primarily at $z \lesssim 1$ (e.g., Chen & Lanzetta 2003), a definitive association with star-forming systems or Lyman break galaxies (LBGs) remains elusive.

Despite the observational challenges, the various galaxy surveys have provided evidence for near solar metallicities in at least some of the bright high-redshift galaxies (Shapley et al. 2004; Swinbank et al. 2004). Typical star formation rates in the bright galaxies are in the range of ~ 10–$10^2\ M_\odot\ yr^{-1}$ (Shapley et al. 2001; Förster Schreiber et al. 2004; Swinbank et al. 2004). On the other hand, DLAs appear to be metal-poor, with a typical $Z \sim 0.03\ Z_\odot$ (Prochaska et al. 2003), and while they exhibit evidence for star formation in a few cases, the rates typically appear to be lower than in the LBGs (Bunker et al. 1999).

An alternative approach to probing the intervening gas in galaxies and the IGM is to use the afterglows of gamma-ray bursts (GRBs). In the context of the relation to star formation and the nature of DLAs, GRBs offer several advantages over quasar studies. First, GRBs are embedded in star-forming galaxies, with typical offsets of a few kiloparsecs or less (Bloom et al. 2002). They therefore not only provide a direct link to star formation but also probe the regions of most intense star formation, and hence the production and dispersal of metals. Second, since the GRB afterglow emission fades away on a timescale of days to weeks, the host galaxy and any intervening DLAs can be subsequently studied directly (e.g., Vreeswijk et al. 2004).

Third, and perhaps most important, since GRBs are likely to be located in star-forming regions (e.g., molecular clouds) within

[1] Observatories of the Carnegie Institution of Washington, 813 Santa Barbara Street, Pasadena, CA 91101.

[2] Princeton University Observatory, Peyton Hall, Ivy Lane, Princeton, NJ 08544.

[3] Hubble Fellow.

[4] Pomona College Department of Physics and Astronomy, 610 North College Avenue, Claremont, CA 91711.

[5] Space Radiation Laboratory, Mail Stop 220-47, California Institute of Technology, Pasadena, CA 91125.

[6] Division of Physics, Mathematics, and Astronomy, Mail Stop 105-24, California Institute of Technology, Pasadena, CA 91125.

[7] Department of Astronomy and Astrophysics, Pennsylvania State University, 525 Davey Laboratory, University Park, PA 16802.
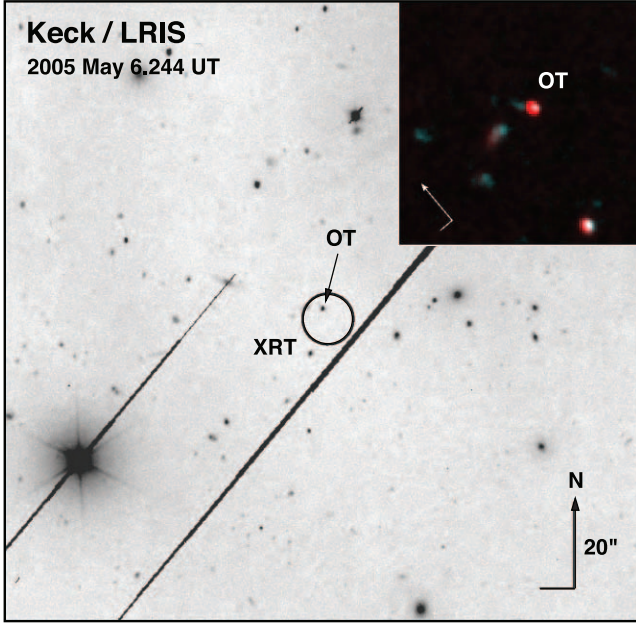
FIG. 1.—Discovery image of the optical afterglow of GRB 050505 obtained with LRIS on the Keck I 10 m telescope. The inset is a combined $g + I$ flux-calibrated color image clearly showing the red color of the afterglow, which is due to the damped Lyα absorption, the Lyα forest, and the Lyman limit absorption at $\lambda \lesssim 4900$ Å (see Fig. 2).

their host galaxies, this approach provides the only systematic way to directly probe the small-scale environment and conditions of star formation at high redshift; the probability of intersecting an individual molecular cloud in a quasar sight line is vanishingly small. In the same vein, GRBs can probe the circumstellar environment of the progenitor star itself and provide a unique view of the mass-loss history and properties of the progenitor (e.g., metallicity, mass, binarity). With a large statistical sample, this is the only way to compare the properties of massive stars and individual star-forming regions at high redshift to those in the Milky Way and the local universe.

Over the past few years, several absorption spectra of GRB afterglows have been obtained, revealing relatively large neutral hydrogen column densities (most in the DLA category; e.g., Vreeswijk et al. 2004). The metallicity, inferred in only a few cases, appears to be subsolar ($Z \sim 0.01–0.1 \, Z_\odot$; Vreeswijk et al. 2004; Chen et al. 2005; Starling et al. 2005a) but with a larger dust content than in QSO-DLAs (Savaglio et al. 2003). In addition, some spectra reveal complex velocity structure, interpreted as arising from ordered galactic rotation (Castro et al. 2003) and in one case appearing to arise in the complex wind environment of the progenitor star (e.g., Möller et al. 2002). These results already suggest that GRBs probe environments that are likely missed in the quasar surveys.

With the advent of the *Swift* satellite, we can now start to use GRBs as probes of the high-redshift universe in a systematic manner. *Swift*'s sensitivity and ability to rapidly and accurately localize a large number of GRBs have resulted in a redshift distribution spanning nearly uniformly from $z \sim 0.5$ to $\gtrsim 6$ (Berger et al. 2005; Jakobsson et al. 2006; Kawai et al. 2005; Haislip et al. 2005). This sample is therefore well matched to the star formation history of the universe and over time will allow us to address the redshift evolution of star-forming environments and perhaps individual massive stars.

Along these lines, we present here an absorption spectrum of GRB 050505, which reveals a DLA with a column density

$\log N(\mathrm{H\,I}) = 22.05 \pm 0.10$ at a redshift of $z = 4.2748$. This system is currently the highest redshift GRB host for which detailed information is available. The spectrum probes not only the interstellar medium of the host galaxy but also provides information on the local environment of the burst, likely including the wind of the progenitor star from which we are able to draw conclusions about the nature of the star that exploded.

2. OBSERVATIONS

GRB 050505 was detected by *Swift* on 2005 May 5.974 UT. The duration and fluence of the burst were 60 s and $(4.1 \pm 0.4) \times 10^{-6}$ ergs cm^{-2}, respectively (Hullinger et al. 2005). Observations with the *Swift* X-ray telescope (XRT) started 47 minutes after the burst and revealed an uncataloged source at $\alpha = 09^{\mathrm{h}}27^{\mathrm{m}}03^{\mathrm{s}}.2$, $\delta = +30°16'21''.5$ (J2000.0) with an uncertainty of about $6''$ and a flux of $\sim 2 \times 10^{-11}$ ergs cm^{-2} s^{-1} (Kennea et al. 2005). No object was detected by the *Swift* UV/optical telescope (UVOT) in the first 8 hr to a limit of $V > 20.35$ and $B > 21.04$ mag, at a mean time of 2.49 and 2.59 hr, respectively (Rosen et al. 2005).

We initiated observations of GRB 050505 with the Low Resolution Imaging Spectrometer (LRIS) mounted on the Keck I 10 m telescope about 6.4 hr after the burst. We obtained simultaneous g- and I-band observations and detected an object close to the center of the XRT error circle at $\alpha = 09^{\mathrm{h}}27^{\mathrm{m}}03^{\mathrm{s}}.3$, $\delta = +30°16'23''.7$ (J2000.0), with a brightness $I = 20.51 \pm 0.05$ and $g = 23.67 \pm 0.12$ mag (Fig. 1). The spectral slope between the two bands, $F_\nu \propto \nu^{-4.9 \pm 0.3}$, is too sharp for host galaxy extinction and instead suggests a redshift $z \sim 4–5.5$. Contemporaneous observations with UKIRT revealed a near-IR counterpart with a brightness of $K = 18.1 \pm 0.2$ mag (Rol et al. 2005).

Following the identification of the afterglow we used LRIS to obtain two 900 s spectra with a $1''$ wide slit (Fig. 2). The spectra were reduced using standard IRAF routines, while rectification and sky subtraction were performed using the method of Kelson (2003). Wavelength calibration was performed using HgArNeZnCd arc lamps, and air-to-vacuum and heliocentric
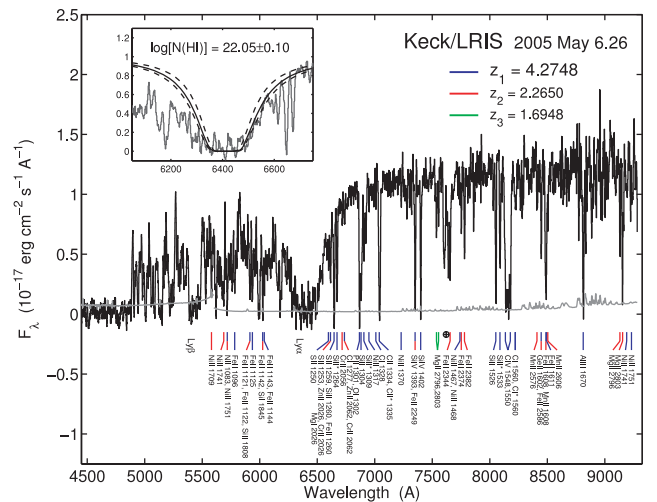

FIG. 2.—Absorption spectrum of GRB 050505 obtained with LRIS on the Keck I 10 m telescope. Observational details are given in § 2. Metal absorption features from all three systems are shown, including lines that are blends from both z_1 and z_2. We note that absorption features blueward of the damped Lyα feature are strongly blended with the Lyα forest at the resolution of our spectrum and their position is shown only for completeness. The inset shows a zoom-in of the Lyα absorption. The solid line is the best fit with $\log N(\mathrm{H\,I}) = 22.05$, and the dashed lines designate the 1 σ uncertainty of 0.1 dex.

corrections were applied. The resulting dispersion scales are 1.86 Å pixel^{-1} for the red side and 0.61 Å pixel^{-1} for the blue side, with an rms wavelength uncertainty of about 0.2 Å. Finally, flux calibration was performed using the spectrophotometric standard BD +28 4211, with a correction for the small amount of Galactic extinction, $E(B - V) = 0.021$ mag (Schlegel et al. 1998). Convolution of the spectrum with the I-filter bandpass results in a flux density of 15.8 ± 1.5 μJy (20.5 ± 0.1 mag), in very good agreement with the measured I-band magnitude. This indicates that slit losses were minimal.

We identify three redshift systems in the extracted spectrum, $z_1 = 4.2748 \pm 0.0008, z_2 = 2.2650 \pm 0.0008$, and $z_3 = 1.6948 \pm 0.0003$. We associate the redshift system z_1 with the host galaxy of GRB 050505, given the nature of the absorption lines (see § 3) and the lack of Lyα forest absorption redward of the damped Lyα feature at the redshift z_1. At this redshift, using the standard cosmology ($H_0 = 71$ km s^{-1} Mpc^{-1}, $\Omega_m = 0.27$, and $\Omega_\Lambda = 0.73$), the isotropic-equivalent γ-ray energy release is $E_{\gamma,\mathrm{iso}} \approx 8.9 \times 10^{53}$ ergs, while the X-ray luminosity extrapolated to $t = 10$ hr (assuming the typical $F_\nu \propto t^{-1.3}$) is $L_{X,\mathrm{iso}} \approx 2.3 \times 10^{46}$ ergs s^{-1} (Nousek et al. 2005). Both values are at the high end of the distribution for previous GRBs (Berger et al. 2003; Bloom et al. 2003).

3. THE HOST GALAXY ABSORPTION SYSTEM

The spectrum of GRB 050505 is dominated by a broad absorption feature centered on an observed wavelength of about 6400 Å, which we identify as Lyα. A Voigt profile fit to the Lyα absorption feature results in a column density of neutral hydrogen, $\log N(\mathrm{H\,I}) = 22.05 \pm 0.10$, indicating that the absorber is a DLA, with one of the highest column densities measured to date in either QSO or GRB sight lines (Curran et al. 2002; Vreeswijk et al. 2004). We note that the actual column density may be somewhat higher, since, unlike in the case of quasars, the GRB is embedded in the host galaxy of the DLA (Vreeswijk et al. 2004). The average flux decrement between Lyα and Lyβ is about 0.55, which is in good agreement with the values measured in quasar sight lines at the same redshift (Cristiani et al. 1993).

Blueward of the damped Lyα feature we detect absorption from the Lyα forest, likely mixed with metal absorption features of oxygen, silicon, nitrogen, sulfur, carbon, and iron. Due to the low resolution of our spectrum we cannot disentangle the contribution of the metals from the forest. We also detect Lyβ absorption, and at a wavelength of about 4880 Å we detect the Lyman limit.

Redward of the Lyα absorption feature we detect a wide range of metal lines. The identifications, observed wavelengths, and equivalent widths (EWs) of these lines are listed in Table 1. We note that in some cases these lines are blended with absorption features from the lower redshift system at $z_2 = 2.265$. Most of the lines detected in the spectrum appear to be saturated. We can obtain a lower limit on the column density assuming the optically thin case

$$N = \frac{m_e c^2}{\pi e^2} \frac{W_\lambda}{f \lambda^2} = 1.13 \times 10^{20} \text{ cm}^{-2} \, \frac{(W_\lambda / \text{Å})}{(\lambda / \text{Å})^2 f}, \qquad (1)$$

where f is the oscillator strength, W_λ is the EW, and λ is the rest wavelength. The resulting lower limits for each transition are listed in Table 1.

Since most of the lines are saturated and therefore do not lie on the linear part of the curve of growth (COG), we construct a joint COG for all the detected transitions that do not suffer from strong blending. In this case we use the standard formulation (Spitzer 1978),

$$W_\lambda = \frac{2bF(\tau_0)\lambda}{c}, \qquad (2)$$

where the line center's optical depth is given by

$$\tau_0 = \frac{\pi^{1/2} e^2 f \lambda N}{m_e c b} = 1.496 \times 10^{-15} \frac{f(\lambda/\text{Å})N}{(b/\text{km s}^{-1})} \qquad (3)$$

and the function

$$F(\tau_0) = \int_0^\infty \left[1 - \exp\left(-\tau_0 e^{-x^2}\right) \right] dx. \qquad (4)$$

We assume that all species share the same value of the Doppler parameter, b, and we fit iteratively for b and the column density of each species (e.g., Savaglio et al. 2003). The resulting best-fit COG is shown in Figure 3, and the column densities are listed in Table 2. We find that lines of C I and Ni II are well described by the linear part of the COG, lines of S II are mildly saturated, and most other species lie on the flat portion of the COG. We stress that given the assumption of a single b-value, as well as the low resolution of our spectrum, the derived column densities of the strongly saturated lines should still be considered as rough lower limits.

With this caveat in mind we derive the following abundances from the COG analysis. The column density of S II is $\log N \approx 16.1$, leading to an abundance relative to the solar value of $[\mathrm{S/H}] \approx -1.2$; here we use the compilation of solar abundances of Asplund et al. (2005). Sulfur is a nonrefractory element and its gas-phase abundance therefore closely matches the gas metallicity. The derived value is roughly similar to those of both QSO- and other GRB-DLAs. The Fe II column density of $\log N \approx 15.5$ indicates an abundance of $[\mathrm{Fe/H}] \approx -2.0$, which is similar to the mean value for QSO-DLAs at a similar redshift range (e.g., Prochaska et al. 2003). The ratio of sulfur to iron, $[\mathrm{S/Fe}] \approx 0.8$, however, is at the high end of values measured for QSO-DLAs, which at $[\mathrm{Fe/H}] \approx -2.0$ range from about 0.1 to 1 (Lopez & Ellison 2003). Since iron is a strongly depleted element, the large value of $[\mathrm{S/Fe}]$ suggests a high dust content, similar to the inference made in several other GRB-DLAs (Savaglio et al. 2003; Savaglio & Fall 2004; Watson et al. 2005).

Inspecting the abundances of other ions, we find that $[\mathrm{Si/H}] \approx -1.6$ when we sum the contributions of Si II and Si IV. The ratio compared to iron is $[\mathrm{Si/Fe}] \approx 0.4$, which is in excellent agreement with the median value of about 0.4 for QSO-DLAs (Wolfe et al. 2005).

Using the abundances of sulfur, silicon, and iron, in Figure 4 we provide a comparison to the Milky Way depletion patterns. We consider the four typical patterns of warm halo (WH), warm disk+halo (WDH), warm disk (WD), and cool disk (CD) clouds (Savage & Sembach 1996) and follow the method of Savaglio et al. (2003) to determine the metallicity and dust-to-gas ratio in each case. We find that the first three depletion patterns provide an adequate representation of the data with a metallicity $Z \approx 0.06\,Z_\odot$ and dust-to-gas ratios of 1.1 (WH), 0.95 (WDH), and 0.85 (WD). The cool disk depletion pattern does not provide an adequate fit, since it underestimates the silicon abundance and overestimates the iron abundance. Given the inferred metallicities and dust-to-gas ratios we calculate a rest-frame V-band extinction of about 0.3 ± 0.1 mag.

TABLE 1
Line Identification

$\lambda_{\rm obs}$ (Å) (1)	Line (Å) (2)	f_{ij} (3)	z (4)	W_0 (Å) (5)	$\log N$ (cm^{-2}) (6)
6597.80....................	S II 1250.584	5.453×10^{-3}	4.2758	0.72	16.0
6614.47....................	S II 1253.811	1.088×10^{-2}	4.2755	1.27	15.9
	Zn II 2026.136	0.489	2.2646	...	...
	Cr II 2026.269	4.710×10^{-3}	2.2644	...	...
	Mg I 2026.477	0.112	2.2640	...	...
6646.34....................	S II 1259.519	1.624×10^{-2}	4.2769	2.60	16.1
	Si II 1260.422	1.007	4.2731	...	14.3
	Fe II 1260.533	2.500×10^{-2}	4.2726	...	15.9
6671.86....................	Si II* 1264.738	0.903	4.2753	1.65	14.1
6736.97....................	C I 1277.245	9.665×10^{-2}	4.2747	0.51	14.6
	Cr II 2062.234	7.800×10^{-2}	2.2668	...	...
	Zn II 2062.664	0.256	2.2661	...	...
6866.63[a]....................	O I 1302.168	4.887×10^{-2}	4.2732	1.51	15.3
6880.58[a]....................	Si II 1304.370	9.400×10^{-2}	4.2750	3.25	15.4
6905.64[a]....................	Si II* 1309.275	8.600×10^{-2}	4.2744	1.07	14.9
6921.57[a]....................	?	...	...	...	...
6949.48....................	Ni II 1317.217	7.786×10^{-2}	4.2759	0.22	14.3
7009.27....................	C I 1328.833	5.804×10^{-2}	4.2748	0.37	14.6
7040.95....................	C II 1334.532	0.128	4.2760	3.37	15.2
	C II* 1335.708	0.115	4.2713	...	15.3
7350.47....................	Si IV 1393.755	0.528	4.2739	1.77	14.3
	Fe II 2249.877	1.821×10^{-3}	2.2671	...	...
7399.07....................	Si IV 1402.770	0.262	4.2746	1.60	14.5
7536.67....................	Mg II 2796.352	0.612	1.6952	1.98	13.7
7554.21....................	Mg II 2803.531	0.305	1.6945	0.94	13.7
7604.14....................	⊕	...	...	...	...
7625.86[b]....................	⊕	...	...	...	...
7639.15[b]....................	?	...	...	...	...
7654.06[b]....................	Fe II 2344.214	0.114	2.2651	2.29	14.6
7676.48[b]....................	Ni II 1454.842	3.230×10^{-2}	4.2765	1.36	15.4
7740.67....................	Ni II 1467.259	6.300×10^{-3}	4.2756	0.25	15.3
	Ni II 1467.756	9.900×10^{-3}	4.2738	...	15.1
7752.13....................	Fe II 2374.461	3.130×10^{-2}	2.2648	0.87	14.7
7779.65....................	Fe II 2382.765	0.320	2.2650	1.52	14.0
8030.42....................	?	...	...	...	...
8051.97....................	Si II 1526.707	0.127	4.2741	1.81	14.8
8088.55....................	Si II* 1533.432	0.132	4.2748	1.58	14.8
8104.98....................	?	...	...	...	...
8138.73....................	C IV 1548.195	0.191	4.2569	3.23	14.9
8151.23....................	C IV 1550.770	9.522×10^{-2}	4.2562	2.99	15.2
8164.63....................	C IV 1548.195	0.191	4.2736	2.69	14.8
8177.95....................	C IV 1550.770	9.522×10^{-2}	4.2735	2.64	15.1
8221.83....................	C I 1560.309	8.041×10^{-2}	4.2694	1.39	14.9
	C I* 1560.682	6.030×10^{-2}	4.2681	...	15.0
	C I* 1560.709	2.010×10^{-2}	4.2680	...	15.5
8411.32....................	Mn II 2576.877	0.351	2.2642	0.95	13.7
8446.68....................	Fe II 2586.650	6.910×10^{-2}	2.2655	1.70	14.6
8487.59....................	Fe II 1608.451	5.800×10^{-2}	4.2769	2.73	15.3
	Fe II 2600.173	0.239	2.2642	...	...
8505.42....................	Fe II 1611.200	1.360×10^{-3}	4.2789	0.54	16.2
	Mn II 2606.462	0.193	2.2632	...	...
8811.67....................	Al II 1670.787	1.880	4.2740	2.55	13.7
9131.04....................	Mg II 2796.352	0.612	2.2653	1.74	13.6
9155.12....................	Mg II 2803.531	0.305	2.2656	2.10	14.0
9162.51....................	?	...	...	...	...
9189.78....................	Ni II 1741.553	4.270×10^{-2}	4.2768	0.91	14.9

Notes.—Absorption features identified in the spectrum of GRB 050505. We do not include metal lines blueward of the Lyα absorption since at the low resolution of our spectrum these lines are blended with Lyα forest features. Col. (1): observed wavelength; col. (2): line identification; col. (3): oscillator strength (Prochaska et al. 2003); col. (4): redshift of the line; col. (5): rest-frame EW; and col. (6): logarithm of the column density assuming the optically thin case (eq. [1]); in most cases this is a lower limit since the lines are generally saturated. In the case of blended features we derive the column density by assuming that the total EW is due to the highest redshift feature (typically the host galaxy).

[a] Absorption features are located in the atmospheric B band.

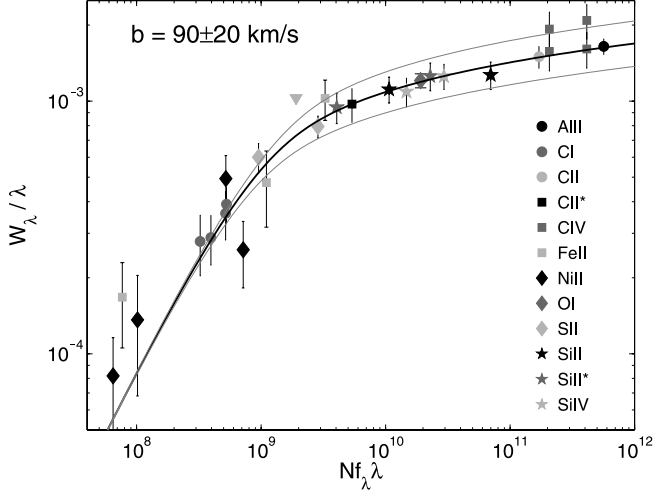[b] Absorption features are located in the atmospheric A band.

FIG. 3.—COG for the host galaxy system of GRB 050505. We constructed the COG by iteratively fitting for the column densities of individual ions and the Doppler parameter, b, which we assumed to have a single value. Transitions in the linear part of the COG lead to well-determined columns (modulo the low resolution of our spectrum). Transitions on the flat portion of the COG are sensitive to the value of b and should be considered as lower limits.
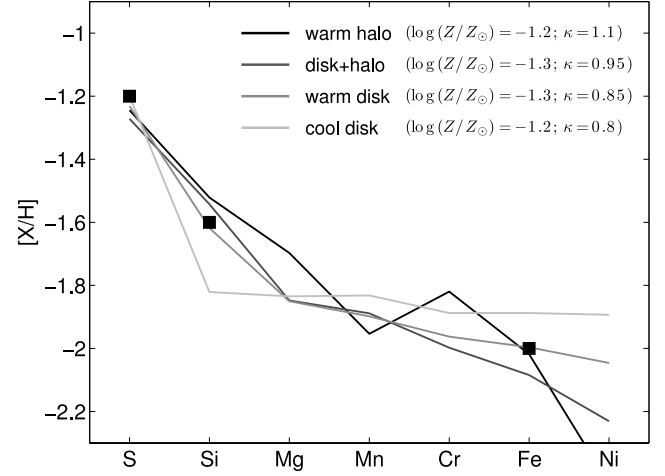

FIG. 4.—Depletion pattern for the host galaxy of GRB 050505 using the inferred columns of sulfur, silicon, and iron relative to hydrogen. The lines represent the depletion patterns expected for various phases of the interstellar medium based on observations in the Milky Way (Savage & Sembach 1996), with the dust-to-gas (κ) and metallicity left as free parameters. We find that a cool disk interpretation is unlikely.

3.1. A C IV Outflow

The most prominent metal absorption feature in the spectrum of GRB 050505, with a total rest-frame EW of about 11.6 Å, is a blend of C IV $\lambda\lambda$1548, 1550. The overall velocity spread of this feature is about 950 km s^{-1}, extending blueward of the systemic redshift of the host galaxy, as defined by other metal absorption features (Fig. 5). The wide velocity spread is not observed in any of the other low- or high-ionization features; for example, the limit on blueshifted Si IV is $\log N < 13.5$, at least a factor of 30 below the C IV column density. It is not clear from the low-resolution spectrum whether the velocity structure is due to a set of discrete absorbers or to a relatively uniform distribution of C IV.

Regardless of this distinction, the observed velocity range is much larger than the typical values associated with the rotation or velocity dispersion of individual galaxies, including those

TABLE 2
COLUMN DENSITIES OF IONS IN z_1

Ion	$\log N$ (cm^{-3})	[X/H]
H I	22.05	...
C I	14.6	−3.8
C II	17.0	−1.4
C IV	17.1	−1.3
O I	16.5	−2.2
Al II	16.3	−0.3
Si II	15.7	−1.8
Si II*	15.1	−2.4
Si IV	15.6	−2.0
S II	16.1	−1.2
Fe II	15.5	−2.0
Ni II	14.6	−1.7

NOTES.—Ionic column densities and abundances relative to the solar values as derived from the curve-of-growth analysis (Fig. 3). These values are lower limits in most cases given the low spectral resolution and the location of most lines on the flat portion of the COG. Thus, the metallicity as inferred from the sulfur abundance is $\gtrsim 0.06\ Z_\odot$.
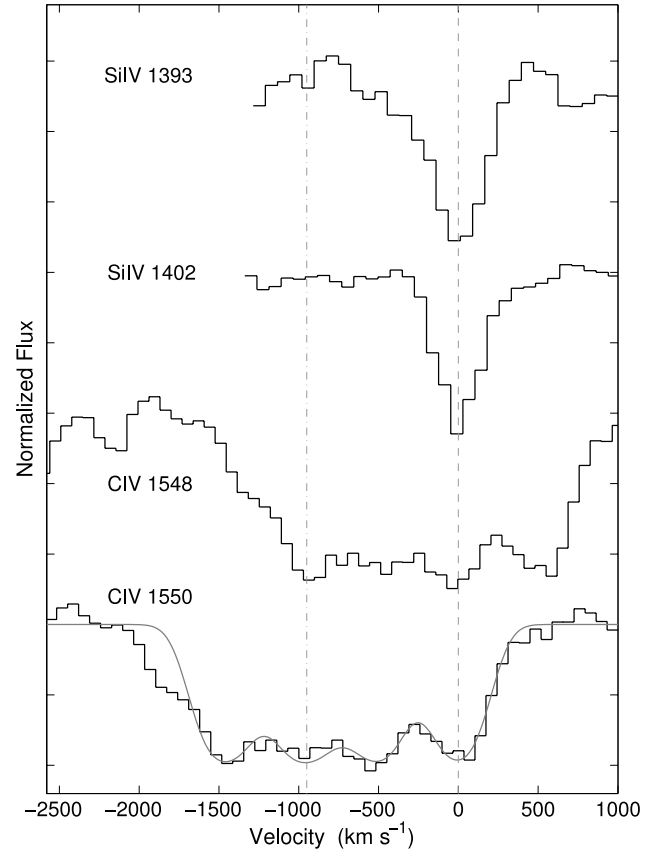

FIG. 5.—Absorption features of C IV and Si IV. The C IV doublet exhibits a velocity spread of about 1000 km s^{-1}, which is not detected in Si IV. The gray line shows the expected absorption profile from two systems at $z_{1A} = 4.2741$ and $z_{1B} = 4.2572$ with C IV column densities of 1 and 2×10^{15} cm^{-2}, respectively, and $b = 90$ km s^{-1} (see Fig. 3). This scenario provides an adequate fit to the data and indicates that the velocity structure is most likely due to a fast wind from the progenitor star.

observed in past GRB absorption spectra (e.g., GRB 000926 with $v \approx 170$ km s^{-1}; Castro et al. 2003). Similarly, blueshifted absorption by interstellar low- and high-ionization gas has been detected in the stacked spectra of LBGs, but with a typical velocity shift relative to the nebular emission lines of only about -150 km s^{-1} (Adelberger et al. 2003). On the other hand, Frye et al. (2002) find evidence for outflows in $z \gtrsim 4$ lensed galaxies that approach 800 km s^{-1}, but these outflows are evident in low-ionization lines of O I, Si II, and C II. In local bright starburst galaxies outflow velocities are typically $\lesssim 300$ km s^{-1} (Heckman et al. 2000). Therefore, unless the wind from the host galaxy of GRB 050505 is unusually fast, we consider this interpretation unlikely. This would particularly be the case if the host of GRB 050505 is similar to those of other GRBs, which tend to have relatively low masses (Christensen et al. 2004) and would therefore have escape velocities much smaller than 10^3 km s^{-1}.

The C IV absorption may be alternatively related to an extended large-scale structure along the line of sight. Adelberger et al. (2003) find a strong correlation between the location of C IV absorbers in quasar sight lines and the location of LBGs. In particular, for a C IV column density of $>10^{14}$ cm^{-2} (as observed in the spectrum of GRB 050505) about 80% of the absorbers lie within 600 km s^{-1} and $\Delta\theta = 35''$ of an LBG. While this velocity range is similar to the one observed here, it has been argued that the actual outflow velocities are $\lesssim 400$ km s^{-1} (Songaila 2006) and that the extent of the C IV bubbles may be a reflection of pregalactic enrichment at $z \sim 10$ by slower winds from dwarf galaxies (Porciani & Madau 2005). Since here we directly detect an outflow with $v \sim 10^3$ km s^{-1}, it is unlikely to be related to the C IV bubbles discussed in Adelberger et al. (2003) and Songaila (2006).

Another possibility in the context of an extended structure is that the C IV absorption arises from an overlapping structure of galactic halos, perhaps stretched out along a dark matter filament. This hypothesis is difficult to assess with a single absorption spectrum. However, if such structures are ubiquitous they should be observed in a large fraction of GRB absorption spectra, as well as in quasar absorption spectra. Studies of C IV systems in quasar spectra suggest that these systems are strongly clustered for velocity shifts of $\lesssim 200$ km s^{-1} and are essentially uncorrelated for $v \gtrsim 500$ km s^{-1} (Rauch et al. 1996; Pichon et al. 2003). Thus, we conclude that the observed C IV velocity structure is not due to a galactic-scale phenomenon.

In the context of a massive star progenitor, an attractive alternative is that the C IV velocity structure is the signature of a fast wind. A similar inference was made in the case of GRB 021004, which exhibited a complex velocity structure extending from about 140 to 3000 km s^{-1} (Möller et al. 2002; Mirabal et al. 2003; Schaefer et al. 2003; Fiore et al. 2005; Starling et al. 2005b). The presence of such a fast outflow led to the general conclusion that the progenitor was a Wolf-Rayet star. However, unlike in the case presented here, the velocity structure in the spectrum of GRB 021004 was evident in both low- and high-ionization lines, including H I. This raised the difficulty of explaining the presence of both types of species in the highly ionized burst environment, as well as the presence of a large column of hydrogen in a Wolf-Rayet wind, although Starling et al. (2005b) suggest that the latter may be due to the presence of a hydrogen-rich companion.

While these difficulties prevented a definitive explanation of the high-velocity absorbers, two main possibilities have been discussed. Mirabal et al. (2003) argue that to reach the observed expansion velocities, radiative acceleration of the preexisting

fragmented shell nebula is required. In this model the interaction of the fast Wolf-Rayet wind with the slower winds of earlier mass-loss episodes results in a fragmented structure due to Rayleigh-Taylor instabilities. The radiation pressure produced by the GRB and afterglow emission then accelerates the fragmented shell nebula to velocities of hundreds to thousands of kilometers per second.

Van Marle et al. (2005), on the other hand, produce hydrodynamic numerical simulations of the interactions of various mass-loss phases (fast main sequence wind, slow red supergiant wind, and a fast Wolf-Rayet wind) and conclude that these interactions lead to a clumpy structure with a velocity range in excess of 2000 km s^{-1}. The fragmented and clumpy structure of the wind is a common theme in both scenarios, and is used to explain the similar kinematic structure in both the low- and high-ionization lines.

In the case of GRB 050505 the velocity structure is only apparent in C IV, suggesting that a more uniform wind structure is allowed. Still, the effect of the ionizing radiation of the GRB has to be taken into account. Since the recombination timescale is expected to be significantly longer than the lifetime of the GRB (unless the density is $\gtrsim 10^6$ cm^{-3}; Perna & Loeb 1998), we can estimate the size of the ionized region roughly as $r \sim \left(E_{\rm ion} \sigma_{\rm C\,IV} / 4\pi e_{\rm ion, C\,IV} \right)^{1/2} \sim$ few $\times 10^{19}$ cm; here $E_{\rm ion}$ is the total energy in photons that can ionize C IV, $\sigma_{\rm C\,IV} = 1.068 \times 10^{-16}$ cm^2 is the photoionization cross section, and $e_{\rm ion, C\,IV} = 64.5$ eV is the ionization threshold energy. Clearly, a detailed photoionization calculation is required, but we conclude that outside of a few parsecs C IV ions should remain intact. We stress that the minimum radius for survival of Si IV ions is a factor of about 3.5 times smaller than that of C IV, so that the nondetection of outflowing Si IV cannot be simply attributed to photoionization.

Thus, the observations require a fast-moving ($\sim 10^3$ km s^{-1}) wind, enriched in carbon and deficient in silicon, and with a radius of at least a few parsecs. These requirements can be naturally satisfied in the case of a Wolf-Rayet wind, for which typical velocities can easily exceed 10^3 km s^{-1} and extend out to a distance of ~ 20 pc (Abbott 1978; van Marle et al. 2005).

The lack of silicon absorption, with a column density that is at least a factor of 30 lower than that of C IV, provides interesting constraints on the nature of the progenitor. Calculations of theoretical profiles of C IV and Si IV in the winds from a range of massive stars suggest that while strong C IV absorption is nearly always present, the presence of Si IV lines depends sensitively on a star's mass and metallicity (Leitherer & Lamers 1991). Thus, the wind from progenitors with a low mass and metallicity will have negligible Si IV absorption. For example, in the case of a wind from a 25 $M_\odot$ star at the end of core hydrogen burning the ratio of Si IV to C IV matches the observed limit of EW(Si IV)/EW(C IV) < 0.1 for $Z \lesssim 0.1\, Z_\odot$, while for a 60 $M_\odot$ star the theoretical ratio is ~ 0.5 even for $Z = 0.03\, Z_\odot$. These considerations indicate that the progenitor of GRB 050505 was most likely a carbon-rich (WC) Wolf-Rayet star with a relatively low mass ($\lesssim 25\, M_\odot$) and metallicity ($Z \lesssim 0.1\, Z_\odot$).

However, radiatively driven winds follow a mass-loss rate–metallicity relation, $\dot{M} \propto Z^{0.5-0.7}$ (Maeder & Meynet 1988; Leitherer & Lamers 1991), and therefore single stars reach the Wolf-Rayet phase at a higher mass when their metallicity is low; in the Galaxy $M_{\rm WR, min} \approx 25\, M_\odot$, while in the SMC $M_{\rm WR, min} \approx 45\, M_\odot$ (Maeder 1998; Maeder & Meynet 2000). With a metallicity of $\lesssim 0.1\, Z_\odot$ and a mass of only $\sim 25\, M_\odot$, it appears that the progenitor of GRB 050505 was not sufficiently massive to have become a Wolf-Rayet star. It is therefore likely that the
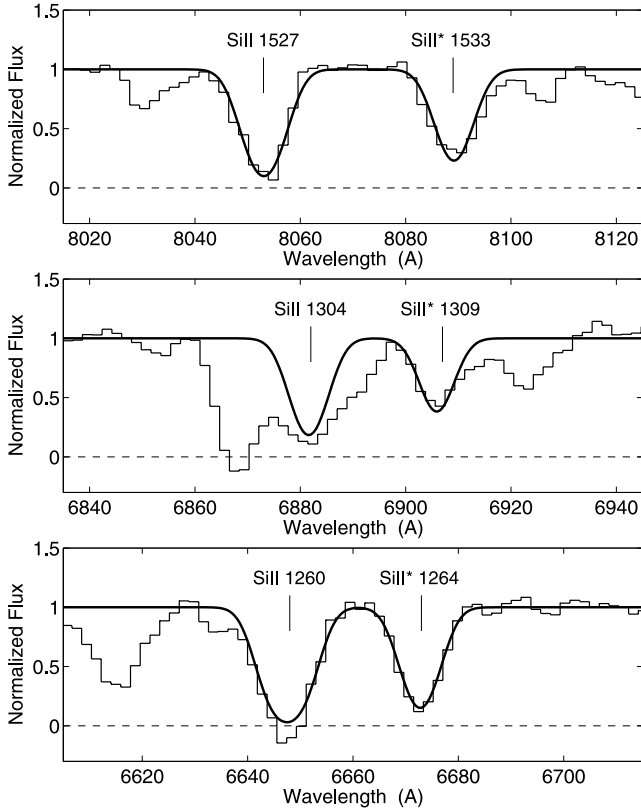
FIG. 6.—Absorption lines of Si II and the fine structure Si II*. The lines of both species appear to be saturated so the ratio of column densities is only roughly determined to be ~0.2. We note that Si II λ1304 and Si II* λ1309 are located in the atmospheric B band and the derived EWs are highly uncertain.

progenitor required a companion star in order to eject the hydrogen envelope.

3.2. Si II*

Another interesting feature of the spectrum of GRB 050505 is the detection of strong fine-structure absorption from Si II*. Since these transitions have not been convincingly detected in QSO-DLAs (e.g., Howk et al. 2005) and since they are most likely excited by collisions with electrons (for $T \lesssim 10^5$ K; Silva & Viegas 2002), we conclude that the Si II* absorber is coincident with the local, high-density environment of the GRB. In Figure 6 we show the three detected Si II and Si II* transitions. We note that the Si II λ1304 and Si II* λ1309 pair is located in the atmospheric B-band, therefore precluding a clear measurement of the EWs. In addition, due to the low spectral resolution, the Si II λ1260 transition is blended with S II λ1259 and Fe II λ1260, although given the large oscillator strength of the Si II transition, it likely dominates the measured EW. Our estimate of the column density is thus based primarily on Si II λ1527 and on Si II* $\lambda\lambda$1264, 1533 (Fig. 6).

The absorption lines of both species are saturated and the ratio of column densities is therefore somewhat uncertain, although it is clear that the column of Si II* is fairly large; using the weakest, unblended line of Si II* under the assumption of the optically thin case, we find $\log N(\text{Si II*}) \approx 14.7$. This value is somewhat higher than those found in two previous GRB spectra: $\log N \approx 14.2$ (GRB 030323; Vreeswijk et al. 2004) and $\log N \approx 14.3$ (GRB 020813; Savaglio & Fall 2004), but the rough similarity may reflect comparable physical conditions in the local environments of GRBs.

Using the COG analysis we find that the ratio of column densities is

$$\frac{N_{\text{Si II*}}}{N_{\text{Si II}}} \approx \frac{10^{15.1}}{10^{15.7}} \approx 0.2. \tag{5}$$

With this value, and using the calculations of Silva & Viegas (2002), we estimate that for a temperature of 10^3 K (i.e., a neutral medium) the implied volume density of H I is $n_{\text{H I}} \sim 10^2$ cm^{-3} if the electron fraction is $n_e = 0.1 n_{\text{H I}}$. If the electron fraction is $n_e < 10^{-4} n_{\text{H I}}$, as may be expected for a neutral medium in which the electrons primarily come from low-ionization species with an abundance relative to hydrogen of $\sim 10^{-4}$ (Silva & Viegas 2002; Vreeswijk et al. 2004), the density is $n_{\text{H I}} \sim 10^4$ cm^{-3}. In this framework, the size of the absorbing region is $\ell \sim 10^{22.05}/10^3 \sim 3.5$ pc assuming that the hydrogen is colocated with the Si II* absorber. The inferred mass of the absorbing region is $M = m_p N(\text{H I})\ell^2 \sim 10^3 M_\odot$. Naturally, if only a fraction of the H I column is associated with the Si II* absorber, then the derived mass and size are in fact upper limits. The inferred compact size of the absorber explains the nondetection of Si II* in the QSO-DLAs, since the probability of intersecting a region of only a few parsecs in size is vanishingly small.

We note that there are two difficulties with this interpretation if we insist that the compact Si II* absorber has to be placed around the GRB. First, in order to survive the burst of ionizing radiation from the GRB (which affects the environment on a scale of ~ 10 pc) the Si II absorber has to be shielded. Second, as discussed in § 3.1, the wind from the progenitor star appears to be deficient in silicon, and another source for the Si II may be required. These arguments suggest that the Si II is located in the vicinity of the GRB, but is probably not directly associated with the progenitor star itself and is instead a signature of the dense environment in the star-forming region.

3.3. *Limits on the* H_2 *Column Density*

Absorption lines of molecular hydrogen may be detected in the spectrum of GRB 050505 if the burst occurred in a dense molecular cloud. Unfortunately, at the low resolution of our spectrum it is essentially impossible to discern H_2 absorption lines from the Lyα forest and transitions due to metals. We note that in general the molecular fraction in DLAs is $\lesssim 10^{-4}$, and only a small number of DLAs exhibit detectable fractions of H_2 (Ledoux et al. 2003). The explanation for this trend is a combination of a low dust content and a fairly intense far-UV radiation field, which combine to reduce the formation rate of H_2 and increase the photodissociation rate, respectively (Wolfe et al. 2005). However, if GRBs tend to occur in molecular clouds, GRB-DLAs may exhibit preferentially higher fractions of molecular hydrogen, particularly in light of the fairly large dust-to-gas ratios in comparison to QSO-DLAs (Savaglio et al. 2003).

On the other hand, as discussed in detail by Draine & Hao (2002), the optical/UV radiation from the GRB itself is expected to photoionize and dissociate H_2 molecules to a distance of a few parsecs. If the cloud hosting the GRB progenitor is smaller than this size or if the burst is located near the edge of the cloud, we expect that no H_2 absorption features will be detected even if the molecular fraction was initially high.

If the cloud is sufficiently large, the UV radiation field is expected to also excite H_2 into vibrational levels that will produce observable absorption features at rest wavelengths of

$1110-1705$ Å (Draine & Hao 2002). The strongest features are at $\lambda = 1254.8$ and 1277.3 Å. While we detect an absorption feature coincident with the 1277.3 Å line, we interpret this feature as C I $\lambda 1277.2$, whose EW is in good agreement with other C I lines. The nondetection of vibrational H_2 absorption, under the assumption that the cloud size is sufficiently large, places a limit of $\log N(H_2^*) \lesssim 18$ cm^{-2} (Draine & Hao 2002), and hence $f(H_2) \lesssim 10^{-4}$.

3.4. *Limits on Lyα Emission*

We do not detect Lyα in emission with a 3 σ limit of $F < 2.1 \times 10^{-17}$ ergs cm^{-2} s^{-1}. At the redshift of the burst this limit translates to an upper limit on the line luminosity of $L < 3.9 \times 10^{42}$ ergs s^{-1}. Using the conversion of Kennicutt (1998) and assuming case B recombination, the limit on the star formation rate implied by the nondetection of Lyα emission is SFR $= 9.1 \times 10^{-43} L_{Ly\alpha} < 3.5\ M_\odot$ yr^{-1}.

The limit on the inferred star formation rate is about a factor of 3 higher than the value inferred for GRB 030323 at $z = 3.372$ (Vreeswijk et al. 2004), but it is significantly lower than the value measured for GRB 021004, $\approx 11\ M_\odot$ yr^{-1}, based on Lyα emission (e.g., Fynbo et al. 2005). In fact, nearly every GRB host in which Lyα emission can be detected has been detected (Jakobsson et al. 2005), while the fraction of LBGs with Lyα EWs similar to those in GRB hosts is only about one-third (Shapley et al. 2003).

We note that the lack of Lyα emission may still accommodate a star formation rate higher than our formal limit, since the Lyα photons are easily destroyed by resonant scattering in the presence of dust. Thus, even for a fairly low dust content it is possible that the star formation rate is in fact higher than the limit provided above. A better assessment of the star formation rate requires near-IR spectroscopy of the host galaxy for detection of Hα at 3.46 μm and/or [O II] $\lambda 3727$ at 1.97 μm.

4. INTERVENING SYSTEMS

We detect two intervening systems at $z_2 = 2.265$ and $z_3 = 1.695$. The latter is detected only in Mg II with a rest-frame EW of 1.98 Å ($\lambda 2796.35$) and 0.94 Å ($\lambda 2803.53$). These values match the expected 2:1 ratio in the optically thin case, suggesting that the lines are not saturated. The derived column density is about 5×10^{13} cm^{-2}. A comparison to the sample of Steidel & Sargent (1992) reveals that $\sim 10\%$ of quasar sight lines reveal systems with similarly large EWs. However, unlike the observed doublet ratio of about two measured here, the range of doublet ratios for the quasar Mg II systems with EW $\gtrsim 2$ Å is typically $1-1.3$, indicative of strong saturation. We finally note that for a magnesium abundance of about 10% the solar value, the inferred column density in the z_3 system suggests an associated neutral hydrogen column density of $\log N(H\ I) \sim 18.5$ cm^{-2}.

The z_2 redshift system exhibits a wider range of absorption features, but, unfortunately, some of these lines are blended with features from the host galaxy. Still, several Fe II lines, as well as the Mg II doublet, and a single Mn II line are not blended, allowing us to estimate the column density of some metals in the z_2 system. A COG fit to the three Fe II lines indicates $b \approx 60$ km s^{-1} and $\log N(Fe\ II) \approx 15.0$. The Mg II ratio of about 0.85 indicates strong saturation and a lower limit on the column density of $\log N(Mg\ II) \approx 14.6$, assuming the same Doppler parameter as for the Fe II lines. Finally, assuming that the single Mn II line is optically thin, we estimate $\log N(Mn\ II) \approx 13.7$. Thus, the relative abundance is $[Fe/Mn] \gtrsim -0.7$, while in DLAs it is typi-
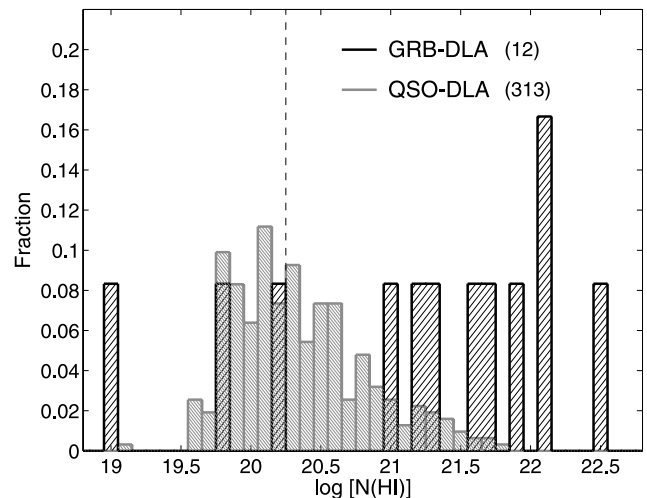
cally ~ 0. This suggests that we may be underestimating the Fe II by about 0.7 dex.

We also note that both iron and manganese are strongly depleted in the Galaxy, while elements such as zinc are relatively undepleted (Savage & Sembach 1996). In our case, the Zn II $\lambda 2062.66$ line is blended with C I from the host galaxy system. However, using the measured EW as an upper limit and assuming the optically thin case, we find $\log N(Zn\ II) < 13.4$. Thus, $[Mn/Zn] > -0.5$ and $[Fe/Zn] > -1.2$ are in agreement with the typical values measured for DLAs of about -0.5 and -0.4, respectively, particularly if the abundance of Fe II is in fact underestimated as suggested above.

5. DISCUSSION AND CONCLUSIONS

The absorption spectrum of GRB 050505 exhibits a DLA with a column density of $\log N(H\ I) \approx 22.05$ associated with the host galaxy. The measured column is higher than that of any QSO-DLA studied to date, but it is similar to those measured for several GRB-DLAs, albeit at the highest redshift to date.[8] In Figure 7 we provide a summary of the column densities measured from both quasars and GRBs to date. As already noted in Vreeswijk et al. (2004), these distributions differ significantly, presumably as a result of the smaller impact parameters in the case of GRB-DLAs and the possibility that they probe individual dense star-forming regions. The metallicity we infer for GRB 050505, $Z \approx 0.06\ Z_\odot$, is within the range of values measured for QSO-DLAs at a similar redshift (Prochaska et al. 2003) but is a factor of several higher than the mean metallicity of about $0.01\ Z_\odot$.

This, along with the metallicities inferred for five additional GRB-DLAs, is shown in Figure 8. In the top panel we plot the metallicity as determined from various indicators as a function of redshift in comparison to QSO-DLAs. For the QSO sample, Prochaska et al. (2003) noted an apparent trend of increased

---

[8] An absorption spectrum of GRB 050904 at $z = 6.29$ has been obtained by Kawai et al. (2005), but the column density and metallicity have not been published so far.
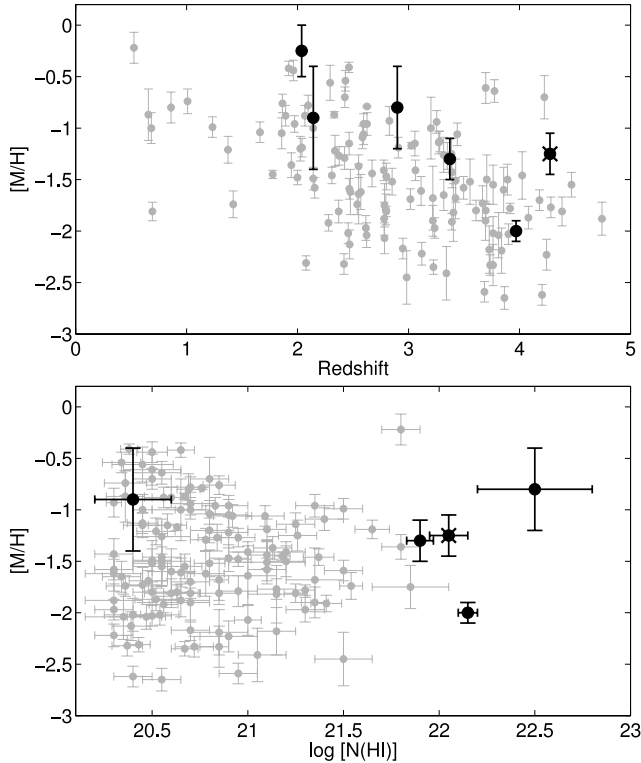
Fig. 8.—*Top*: Metallicity as a function of redshift for QSO-DLAs (*gray*; Prochaska et al. 2003) and GRB-DLAs (*black*; Savaglio et al. 2003; Vreeswijk et al. 2004, 2006; Chen et al. 2005; Starling et al. 2005a; Watson et al. 2005); GRB 050505 is marked with a cross. *Bottom*: Metallicity as a function of neutral hydrogen column density. The trend of increased metallicity with lower redshift, noted for QSO-DLAs by Prochaska et al. (2003), is also apparent in the GRB-DLA sample, albeit at an overall higher metallicity. This suggests that GRBs select more metal-enriched systems, but it is not clear at the present if this is related to the higher column densities.

metallicity with lower redshift. A similar trend appears in the admittedly small GRB-DLA sample, which spans from $z \approx 2$ to 4.3. However, it is also clear that the GRB-DLAs have sys-

tematically higher metallicities compared to QSO-DLAs. In the bottom panel of Figure 8 we plot the metallicity as a function of hydrogen column density. No clear trend is evident, perhaps suggesting that the higher metallicities in GRB-DLAs may not be simply a function of the column density but may reflect a difference in the star formation properties, rates, or history of GRB-selected host galaxies compared to QSO-DLAs.

We highlight two aspects of the spectrum that provide insight into scales and conditions that are not typically probed in quasar sight lines: a C IV outflow that is most likely associated with the wind of the progenitor star, and strong absorption from fine-structure Si II* that is associated with a dense region in the vicinity of the burst. The latter suggests that the GRB progenitor lived in an environment typical of a molecular cloud. The C IV out-flow, taken in association with the lack of corresponding Si IV ab-sorption suggests that the progenitor star had a relatively low mass and metallicity, $M \sim 25\ M_\odot$ and $Z \lesssim 0.1\ Z_\odot$. The combination of these properties suggests that the progenitor was part of a binary system, with the companion responsible for stripping the hydrogen envelope.

The continued detection of high-velocity features in GRB absorption spectra may thus hold the only key to a detailed under-standing of the distribution of progenitor properties (mass, metal-licity, and binarity), as well as the ability to probe the properties of individual molecular clouds at high redshift. Coupled with information on the galactic scale properties of the ISM, GRBs can probe all the scales relevant to our understanding of the star formation process and its relation to metal production, as well as the relation between DLAs and star-forming galaxies.

REFERENCES

Abbott, D. C. 1978, ApJ, 225, 893
Adelberger, K. L., Steidel, C. C., Shapley, A. E., & Pettini, M. 2003, ApJ, 584, 45
Asplund, M., Grevesse, N., & Sauval, A. J. 2005, in ASP Conf. Ser. 336, Cosmic Abundances as Records of Stellar Evolution and Nucleosynthesis, ed. T. G. Barnes III & F. N. Bash (San Francisco: ASP), 25
Berger, E., et al. 2005, ApJ, 634, 501
Berger, E., Kulkarni, S. R., & Frail, D. A. 2003, ApJ, 590, 379
Bloom, J. S., Frail, D. A., & Kulkarni, S. R. 2003, ApJ, 594, 674
Bloom, J. S., Kulkarni, S. R., & Djorgovski, S. G. 2002, AJ, 123, 1111
Bunker, A. J., Warren, S. J., Clements, D. L., Williger, G. M., & Hewett, P. C. 1999, MNRAS, 309, 875
Castro, S., Galama, T. J., Harrison, F. A., Holtzman, J. A., Bloom, J. S., Djorgovski, S. G., & Kulkarni, S. R. 2003, ApJ, 586, 128
Chen, H.-W., & Lanzetta, K. M. 2003, ApJ, 597, 706
Chen, H.-W., Prochaska, J. X., Bloom, J. S., & Thompson, I. B. 2005, ApJ, 634, L25
Christensen, L., Hjorth, J., & Gorosabel, J. 2004, A&A, 425, 913
Cristiani, S., Giallongo, E., Buson, L. M., Gouiffes, C., & La Franca, F. 1993, A&A, 268, 86
Curran, S. J., Webb, J. K., Murphy, M. T., Bandiera, R., Corbelli, E., & Flambaum, V. V. 2002, Publ. Astron. Soc. Australia, 19, 455
Draine, B. T., & Hao, L. 2002, ApJ, 569, 780
Fiore, F., et al. 2005, ApJ, 624, 853
Förster Schreiber, N. M., et al. 2004, ApJ, 616, 40
Frye, B., Broadhurst, T., & Benítez, N. 2002, ApJ, 568, 558
Fynbo, J. P. U., et al. 2005, ApJ, 633, 317
Haislip, J., et al. 2005, Nature, 440, 181

Heckman, T. M., Lehnert, M. D., Strickland, D. K., & Armus, L. 2000, ApJS, 129, 493
Howk, J. C., Wolfe, A. M., & Prochaska, J. X. 2005, ApJ, 622, L81
Hullinger, D., et al. 2005, GCN Circ., 3364
Jakobsson, P., et al. 2004, A&A, 427, 785
———. 2005, MNRAS, 362, 245
———. 2006, A&A, 447, 897
Kawai, N., Yamada, T., Kosugi, G., Hattori, T., & Aoki, K. 2005, GCN Circular, 3937, 1, http://gcn.gsfc.nasa.gov/gcn3/3937.gcn3
Kelson, D. D. 2003, PASP, 115, 688
Kennea, J. A., Burrows, D. N., Hurkett, C. P., Osbourne, J. P., & Gehrels, N. 2005, GCN Circ., 3365
Kennicutt, R. C. 1998, ARA&A, 36, 189
Ledoux, C., Petitjean, P., & Srianand, R. 2003, MNRAS, 346, 209
Leitherer, C., & Lamers, H. J. G. L. 1991, ApJ, 373, 89
Lopez, S., & Ellison, S. L. 2003, A&A, 403, 573
Maeder, A. 1998, in IAU Symp. 189, Fundamental Stellar Properties, T. R. Bedding, A. J. Booth, & J. Davis (Dordrecht: Kluwer), 313
Maeder, A., & Meynet, G. 1988, A&AS, 76, 411
———. 2000, ARA&A, 38, 143
Mirabal, N., et al. 2003, ApJ, 595, 935
Möller, P., et al. 2002, A&A, 396, L21
Nousek, J. A., et al. 2005, preprint (astro-ph/0508332)
Perna, R., & Loeb, A. 1998, ApJ, 501, 467
Pichon, C., Scannapieco, E., Aracil, B., Petitjean, P., Aubert, D., Bergeron, J., & Colombi, S. 2003, ApJ, 597, L97
Porciani, C., & Madau, P. 2005, ApJ, 625, L43

Prochaska, J. X., Bloom, J. S., Wright, J. T., Butler, R. P., Chen, H. W., Vogt, S. S., & Marcy, G. W. 2005a, GCN Circular, 3833, 1, http://gcn.fsfc.nasa.gov/gcn3/3833.gcn3

Prochaska, J. X., Foley, R. J., Chen, H.-W., Bloom, J. S., Hurley, K., Cooper, M., Guhathakurta, R., & Li, W. 2005b, GCN Circular, 3971, 1, http://gcn.fsfc.nasa.gov/gcn3/3971.gcn3

Prochaska, J. X., Gawiser, E., Wolfe, A. M., Cooke, J., & Gelino, D. 2003, ApJS, 147, 227

Rauch, M., Sargent, W. L. W., Womble, D. S., & Barlow, T. A. 1996, ApJ, 467, L5

Rol, E., Tanvir, N., Levan, A., Adamson, A., Fuhrman, L., Priddey, R., & Chapman, R. 2005, GCN Circular, 3372, 1, http://gcn.fsfc.nasa.gov/gcn3/3372.gcn3

Rosen, S., Hurkett, C., Holland, S., Roming, P., Blustin, A., Gehrels, N., Mason, K., & Nousek, J. 2005, GCN Circular, 3371, 1, http://gcn.fsfc.nasa.gov/gcn3/3371.gcn3

Savage, B. D., & Sembach, K. R. 1996, ARA&A, 34, 279

Savaglio, S., & Fall, S. M. 2004, ApJ, 614, 293

Savaglio, S., Fall, S. M., & Fiore, F. 2003, ApJ, 585, 638

Schaefer, B. E., et al. 2003, ApJ, 588, 387

Schlegel, D. J., Finkbeiner, D. P., & Davis, M. 1998, ApJ, 500, 525

Shapley, A. E., Erb, D. K., Pettini, M., Steidel, C. C., & Adelberger, K. L. 2004, ApJ, 612, 108

Shapley, A. E., Steidel, C. C., Adelberger, K. L., Dickinson, M., Giavalisco, M., & Pettini, M. 2001, ApJ, 562, 95

Shapley, A. E., Steidel, C. C., Pettini, M., & Adelberger, K. L. 2003, ApJ, 588, 65

Silva, A. I., & Viegas, S. M. 2002, MNRAS, 329, 135

Songaila, A. 2006, AJ, 131, 24

Spitzer, L. 1978, Physical Processes in the Interstellar Medium (New York: Wiley), 333

Starling, R. L. C., et al. 2005a, A&A, 442, L21

Starling, R. L. C., Wijers, R. A. M. J., Hughes, M. A., Tanvir, N. R., Vreeswijk, P. M., Rol, E., & Salamanca, I. 2005b, MNRAS, 360, 305

Steidel, C. C., Adelberger, K. L., Shapley, A. E., Pettini, M., Dickinson, M., & Giavalisco, M. 2003, ApJ, 592, 728

Steidel, C. C., & Sargent, W. L. W. 1992, ApJS, 80, 1

Swinbank, A. M., Smail, I., Chapman, S. C., Blain, A. W., Ivison, R. J., & Keel, W. C. 2004, ApJ, 617, 64

van Marle, A.-J., Langer, N., & Garcia-Segura, G. 2005, A&A, 444, 837

Vreeswijk, P. M., et al. 2004, A&A, 419, 927

———. 2006, A&A, 447, 145

Watson, D., et al. 2005, preprint (astro-ph/0510368)

Wolfe, A. M., Gawiser, E., & Prochaska, J. X. 2005, ARA&A, 43, 861